How precisely do SPECT images reflect tracer uptake in myocardial infarction? A comparison of thallium-201 and technetium-99m using a myocardial phantom

How Precisely Do SPECT Images Reflect Tracer Uptake in Myocardial Infarction? A Comparison of Thallium-201 and Technetium-99m Using a Myocardial Phantom

Masahisa Onoguchi, Hirotaka Maruno, Teruhiko Takayama and Hajime Murata

Department of Radiological Technology, School of Health Sciences, Faculty of Medicine, Kanazawa University, Kanazawa; Division of Nuclear Medicine, Toranomon Hospital, Tokyo; and National Institute of Radiological Sciences, Chiba, Japan

Objective: We compared the count ratios of ^{201}Tl and ^{99m}Tc on SPECT images and the true radioactivity in a myocardial phantom to study how precisely SPECT images reflect tracer uptake in myocardial infarction.

Methods: A defect with 20%, 40% or 60% of normal myocardial radioactivity was placed in the anterior or inferior wall of a myocardial phantom to simulate myocardial infarction. Lung radioactivity was kept at 10% or 30% of normal myocardial radioactivity. The count ratio on short-axis SPECT images was calculated using the circumferential profile curve analysis.

Results: The count ratios of ^{201}Tl and ^{99m}Tc SPECT images with an anterior wall defect was lower than the true radioactivity in the phantom. The count ratio on SPECT images with the inferior wall defect was greater than the true radioactivity for the 20% and 40% defects and lower for the 60% defect.

Conclusion: SPECT images overestimated decreased perfusion in the anterior wall. SPECT images underestimated decreased perfusion for 20% and 40% perfusion defects in the inferior wall.

Key Words: myocardial phantom; myocardial infarction; single-photon emission computed tomography; thallium-201; technetium-99m

J Nucl Med Technol 1998; 26:252–256

Myocardial perfusion imaging with ^{201}Tl has been used for more than a decade for diagnosing coronary artery disease (CAD). However, this agent has significant disadvantages including low-energy photons of 71 keV and a long physical half-life of 73 hr resulting in decreased overall image resolution. To overcome the disadvantages of ^{201}Tl, ^{99m}Tc heart imaging agents have been developed as an alternative (*1–5*). These agents have several advantages over ^{201}Tl including an ideal 140-keV photopeak for current imaging systems, due to a 6-hr physical half-life a larger amount can be administered to the patient, and simultaneous evaluation of myocardial perfusion and ventricular function is possible. In our clinical experience, we often found that some patients showed a discrepancy between ^{201}Tl and ^{99m}Tc SPECT images in identifying reversible or fixed defects. This might be caused by the differences in the uptake of the radiopharmaceuticals or by differences in detection by current imaging equipment. Therefore, we tried to clarify the differences observed by using a myocardial phantom to simulate various clinical situations.

The purpose of this study was to compare ^{201}Tl and ^{99m}Tc count ratios obtained from SPECT images and the true radioactivity in a phantom to investigate how precisely SPECT images reflect tracer uptake in a myocardial infarction.

MATERIALS AND METHODS

Myocardial Phantom

A myocardial phantom was formed from a polyacrylic cylinder with 10-cm outer and 8-cm inner diameters. It was placed in a body phantom containing the lung, mediastinum and spine (Fig. 1). The compartment corresponding to normal left ventricular myocardium was filled with a homogeneous solution of 140 kBq/ml ^{201}Tl or ^{99m}Tc. A defect was filled with 20%, 40% or 60% of myocardial radioactivity. By rotating the cylinder, the defect was placed in the anterior or the inferior wall. The mediastinum and cylinder were filled with water. The lung field was filled with sawdust, on which ^{201}Tl or ^{99m}Tc was sprayed. Lung radioactivity was kept at 10% or 30% of myocardial radioactivity.

Imaging Protocol

A gamma camera with a low-energy, all-purpose, parallel-hole collimator was used. Thallium-201 and ^{99m}Tc images were acquired at peak energy settings of 71 keV and 140 keV, respectively, with a 20% window. SPECT data were acquired under the same conditions for both ^{201}Tl and ^{99m}Tc. View data were acquired using a zoom factor of 1.33 into a 64 × 64 digital

For correspondence or reprints contact: Masahisa Onoguchi, 5–11-80, Kodatsuno, Kanazawa, Ishikawa, Faculty of Medicine, School of Health Sciences, Kanazawa University, Kanazawa, Japan.

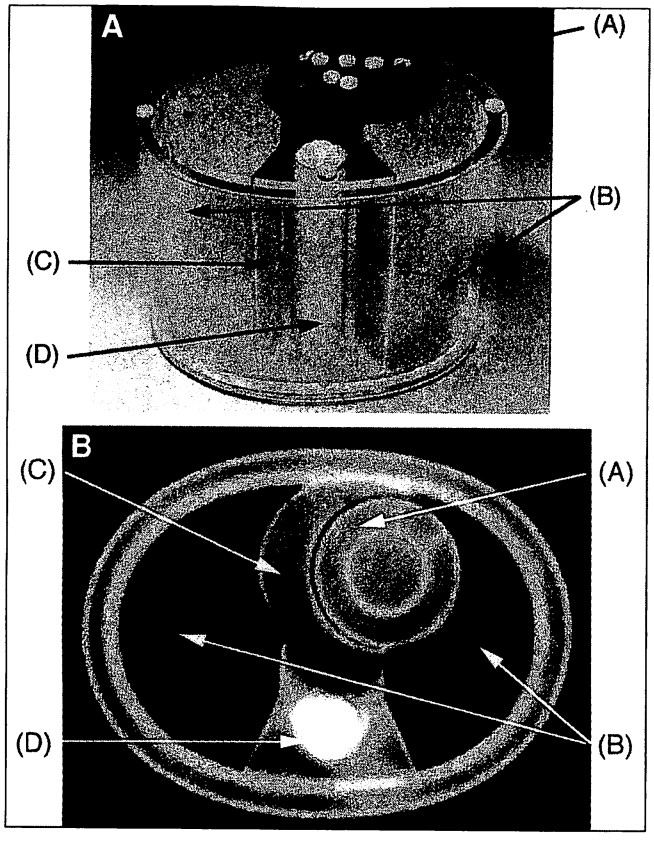

FIGURE 1. (A) Body phantom containing (A arrows) myocardial phantom, (B arrows) lung, (C arrows) mediastinum and (D arrows) spine. (B) X-ray computed tomography image of the body phantom.

matrix (i.e., 4.7 mm/pixel sampling size). Thirty-two projections were obtained for 15 sec each in an 180° arc extending from the 45° right anterior oblique to the left posterior oblique projection (nearly 200 K counts per pixel). All data were prefiltered using a Hanning filter with a cutoff frequency of 0.8 cycles/pixel. Images were reconstructed using a filtered backprojection algorithm and ramp filter with a cutoff frequency of 0 cycles/pixel. No attenuation nor scatter correction was performed. The anterior view image of the SPECT data was regarded as a planar image for calculating lung-to-myocardium ratios.

Data Analysis

The circumferential profile curve was used for analysis. A short-axis image in the middle of the phantom was divided by 40 radii spaced at 9° intervals. The circumferential profile curve was generated by plotting the peak counts per pixel along the radius on a linear graph as a function of angle, the origin of which corresponds to near 8 o'clock position on the SPECT image (Fig. 2). Then each profile curve was normalized to facilitate comparison between the two curves. The activity in the defect was defined as the mean of five segments' activities, while the activity in the normal myocardium was defined as the mean of 35 segments' activities. From these values a defect-to-normal myocardium count ratio (D/N ratio) was calculated for both ^{201}Tl and ^{99m}Tc.

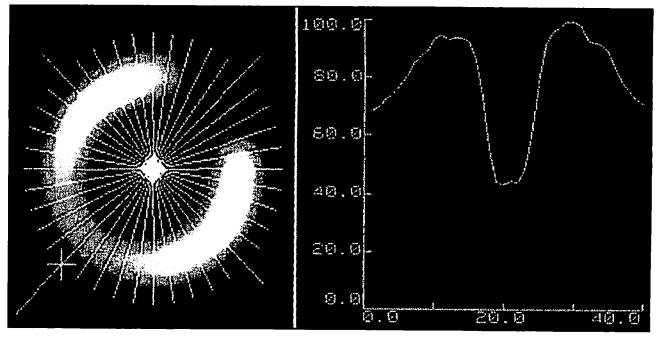

FIGURE 2. A schematic representation of the 360° sampling by 40 radii on a transaxial SPECT image (left) and circumferential profile curve (right).

The lung-to-normal myocardium count ratio (L/M ratio) was calculated using the mean counts/pixel included in the 17 × 18-pixel region of interest (ROI) over the heart and the mean counts/pixel included in the two ROIs of 12 × 18 pixels over the right lung and the 5 × 18 pixels positioned over the left lung in the planar anterior image (Fig. 3).

RESULTS

Comparison of Counting Ratios Between SPECT Images and True Radioactivity in the Phantom

Figure 4 and Table 1 show the comparison of D/N ratios between SPECT images and true radioactivity in the phantom. D/N ratios obtained from SPECT images with the anterior defect were lower than that of true radioactivity for both ^{201}Tl and ^{99m}Tc at 10% and 30% of the L/M ratios. The difference

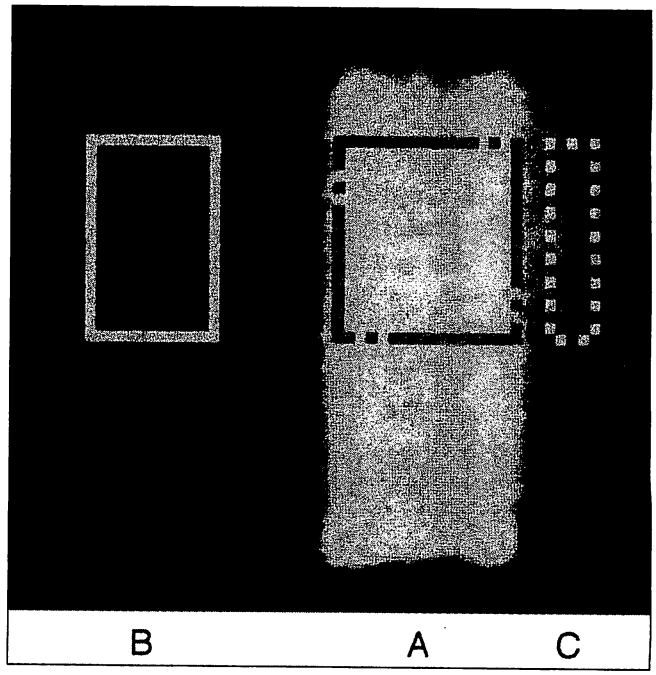

FIGURE 3. Region of interest for the lung-to-myocardium count ratio. (A) 17 × 18 pixels over the heart, (B) 12 × 18 pixels over the right lung, and (C) 5 × 18 pixels over the left lung. Lung count is defined as the mean of counts/pixel included in Regions B and C.

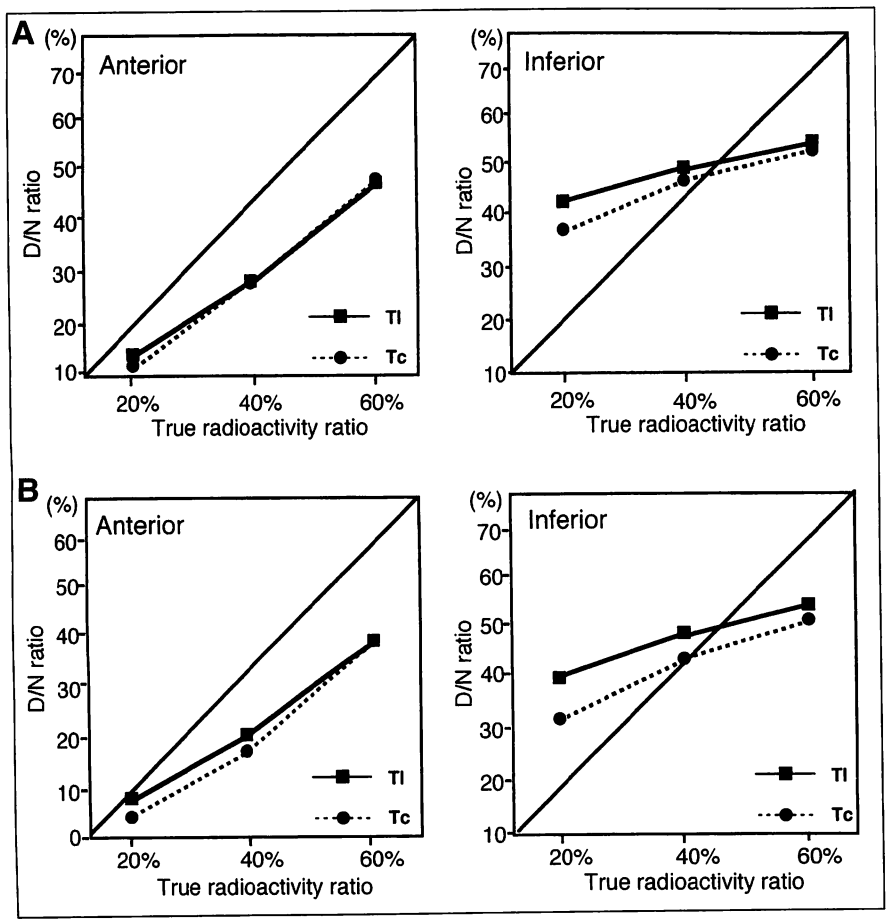

FIGURE 4. Defect-to-myocardium count (D/N) ratios obtained from SPECT images for the anterior (left) and inferior wall (right) defects. D/N ratios with: (A) 10% of lung-to-myocardium count (L/M) ratio; (B) 30% of L/M ratio.

of D/N ratios obtained with both tracers was less than 3.3%. D/N ratios obtained from SPECT images with the inferior defect were greater than true radioactivity for the 20% and 40% defects, while the ratio was lower than the 60% defect. Figure 5 shows examples of short-axis images for different D/N ratios and L/M ratios.

Effect of Lung Radioactivity

Table 2 compares L/M ratios between the anterior planar images and true radioactivity in the phantom. For the 10% of true count ratio, L/M ratios obtained from the planar images were 53.8% and 44.3% for ^{201}Tl and ^{99m}Tc, respectively. Compared with true ratios, the L/M count ratios obtained from the planar images were markedly greater. Similarly, for the 30% of true ratio, L/M ratios obtained from the planar images were 114.6% and 115.5% for ^{201}Tl and ^{99m}Tc, respectively.

DISCUSSION

Many comparative studies for evaluating myocardial perfusion have been performed on ^{201}Tl and ^{99m}Tc heart imaging agents. Rigo et al. (*6*) compared ^{201}Tl *with* ^{99m}Tc-*tetrofosmin* imaging in 40 patients with angiographically proven CAD and documented that there was good segmental correspondence between both tracers for detecting myocardial infarction and ischemia. Cuocolo et al. (*7*) observed an excellent agreement

TABLE 1
Defect-to-Myocardium Count Ratios Obtained from SPECT Images

Radioactivity		L/M ratio: 10%			L/M ratio: 30%		
		^{201}Tl	^{99m}Tc	^{99m}Tc/^{201}Tl	^{201}Tl	^{99m}Tc	^{99m}Tc/^{201}Tl
Anterior defect	60%	44.6%	45.2%	1.01	37.1%	37.1%	1.00
	40%	28.5%	28.5%	1.00	18.4%	14.4%	0.78
	20%	14.9%	11.8%	0.79	7.02%	3.70%	0.53
Inferior defect	60%	52.7%	52.0%	0.99	52.8%	50.6%	0.96
	40%	47.9%	45.4%	0.95	48.2%	42.2%	0.88
	20%	42.6%	37.3%	0.88	38.9%	31.1%	0.80

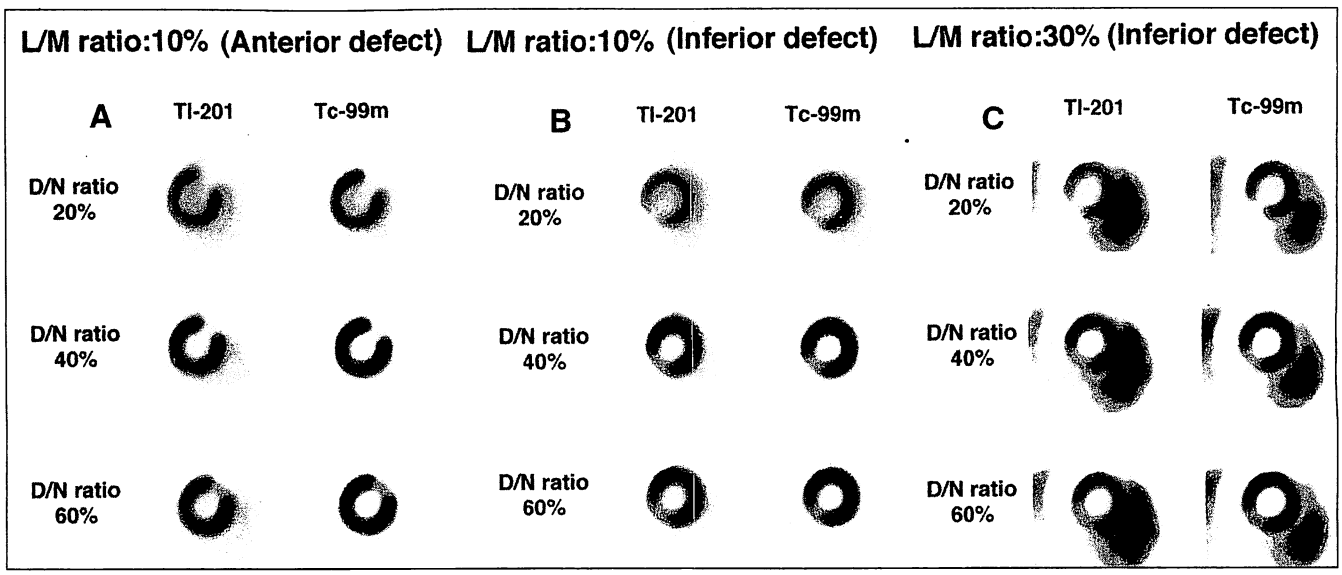

FIGURE 5. Short-axis transaxial images with anterior and inferior wall defects. (A) Anterior wall defect for 10% lung-to-myocardium count (L/M) ratio; (B) inferior wall defect for 10% L/M ratio; and (C) inferior wall defect for 30% L/M ratio.

(90%) for regional uptake between initial ^{201}Tl and resting ^{99m}Tc MIBI images and a decreased agreement (77%) between delayed ^{201}Tl and resting ^{99m}Tc MIBI images. Maurea et al. (*8*) compared rest-injected ^{201}Tl redistribution and resting ^{99m}Tc MIBI myocardial uptake dividing 225 myocardial segments in 15 patients with angiographically proven CAD. Thallium-201 uptake was significantly higher than ^{99m}Tc MIBI uptake in Group 1 (total occlusion), although no significant difference was present in Groups 2 (50%–99% of stenosis) and 3 (< 50% of stenosis). They concluded that ^{201}Tl imaging may identify more accurately the presence of viable myocardium than ^{99m}Tc MIBI imaging. Li et al. (*9*) also have demonstrated that stress/rest ^{99m}Tc MIBI imaging significantly underestimates myocardial viablity. In spite of many clinical studies, there is little phantom data on SPECT imaging with these tracers.

In this study we compared the count ratios of SPECT images with true radioactivity in a phantom. To simulate myocardial infarction, radioactivity in the perfusion defect was decreased to 20%, 40% or 60% of myocardial radioactivity. With the defect in the anterior wall, D/N ratios obtained from SPECT images were lower than the true count ratio. The difference of D/N ratios obtained with both tracers was less than 3.3%. With the defect in the inferior wall, the D/N ratio obtained from SPECT images for ^{201}Tl or ^{99m}Tc was greater than the 20% or 40% of the true count ratio, whereas the D/N ratio was lower than 60% of the true count ratio. Our results suggest that SPECT images underestimate decreased perfusion in the inferior wall, while it overestimates decreased perfusion in the anterior wall. This suggests that radiation originating from the inferior and septal regions is attenuated more than radiation originating from the anterior and lateral walls. Eisner et al. (*10*) studied normal SPECT ^{201}Tl distribution using the bull's-eye display and revealed that the anterior-to-inferior wall count ratios were >1.0 in males but were approximately equal to 1.0 in females and that the septal-to-lateral wall count ratios were <1.0 in both females and males. They presumed that the relative decrease in ^{201}Tl activity in the anterior wall in females and in the inferior wall in males was due to breast tissue attenuation and diaphragmatic attenuation, respectively. Tartagni et al. (*11*) studied the diagnostic accuracy for detecting coronary lesions with both a stress-rest ^{201}Tl study and a dipyridamole ^{99m}Tc MIBI scintigraphy in 30 patients. In their results sensitivity for identifying diseased vessels by ^{201}Tl was 68% for the left anterior descending artery (LAD), 89% for the right coronary artery (RCA), and 80% for the left circumflex artery (LCX) compared to 75%, 89% and 80%, respectively, with ^{99m}Tc MIBI. Specificity was 93% in both cases for LAD, 73% and 63% for RCA, and 53% and 46% for LCX. They concluded that lesions on LAD were identified with a lower sensitivity than those on RCA and LCX. However, they could not provide any explanation for their result of a lower detectability of LAD stenosis. Contrary to their results, Maublant et al. (*12*) compared ^{99m}Tc MIBI myocardial SPECT results for 180° and 360° data collections and demonstrated that the sensitivity was always higher in the anterior than in the inferior lesions, which corresponds to our results. In the quantitative analysis using a circumferential profile curve, Li et al. (*9*) demonstrated that the mean uptake ratio of ^{99m}Tc MIBI in

TABLE 2
Lung-to-Myocardium Count (L/M) Ratios Obtained from Anterior Planar Image

	Anterior planar image L/M ratio	
Radioactivity	^{201}Tl	^{99m}Tc
10%	53.8%	44.3%
30%	114.6%	115.5%

the abnormal regions was 0.53 ± 0.23 (0–0.79) in 27 patients with previous myocardial infarction. Their results support our study design of 20%, 40% and 60% decreased radioactivity in the perfusion defect to simulate clinical states.

Lung radioactivity acts as background on SPECT images. It is important in evaluating the severity of perfusion defects (*13*). In this study, we evaluated the effect of lung radioactivity by simulating lung radioactivity at 10% and 30% of myocardial activity. Sridhara et al. (*14*) reported that the lung-to-heart ratio was 0.5 ± 0.08 at 10 min, and 0.43 ± 0.07 at 4 hr after exercise on ^{201}Tl images. The ratio was 0.38 ± 0.08 and 0.33 ± 0.09 at 5 and 240 min, respectively, after exercise using ^{99m}Tc-tetrofosmin. There was significantly greater lung uptake of ^{201}Tl at exercise. In this study we evaluated the effect of lung radioactivity by simulating lung radioactivity at 10% and 30% of myocardial activity. At 10% of true ratio, L/M ratios from the planar images were 53.8% and 44.3% for ^{201}Tl and ^{99m}Tc, respectively. At 30% of true ratio, they were 114.6% and 115.5% for ^{201}Tl and ^{99m}Tc, respectively. Compared with true ratios, the L/M ratios from the planar images were markedly greater because these results were obtained including the effects of scatter, photon attenuation and background activity. Increased lung uptake can be caused by a variety of pulmonary and cardiac disease states, including ischemic heart disease, congestive heart disease, cardiomyopathy and mitral valve disease (*15*). In cardiac conditions it indicates left ventricular dysfunction. In patients with severe CAD, increased lung radioactivity occurs with exercise as a result of increased pulmonary capillary wedge pressure (*15*). It is reported that the lung-to-myocardium count ratios for ^{201}Tl were 44% in normal subjects and 83% in patients with congestive heart failure (*15,16*).

Many factors should be taken into consideration during analysis of the distribution of radioactivity in the myocardium, including scatter, photon attenuation, background, partial volume effect and the resolution of the imaging procedure. The resolution of a SPECT system is determined by the resolution of the gamma camera including the collimator, spatial and angular sampling, acquisition mode and reconstruction filter. In addition, to evaluate tracer uptake precisely, left ventricular shape, dimensions and wall thickness also should be taken into consideration because of the differences between normal subjects and patients.

CONCLUSION

Careful visual interpretation of infarcted areas on SPECT images is required, especially in patients with inferior infarction. Further investigation is needed on the many factors that affect SPECT images.

REFERENCES

1. Wackers FJ, Berman DS, Maddahi J, et al. Technetium-99m hexakis 2-methoxyisobutyl isonitrile: human biodistribution, dosimetry, safety, and preliminary comparison to thallium-201 for myocardial perfusion imaging. *J Nucl Med* 1989;30:301–311.
2. Sinusas AJ, Beller GA, Smith WH, et al. Quantitative planar imaging with technetium-99m methoxyisobutyl isonitrile: comparison of uptake patterns with thallium-201. *J Nucl Med* 1989;30:1456–1463.
3. Baillet GY, Mena IG, Kuperus JH, et al. Simultaneous technetium-99m MIBI angiography and myocardial perfusion imaging. *J Nucl Med* 1989;30: 38–44.
4. Villanueva-Meyer J, Mena I, Narahara KA. Simultaneous assessment of left ventricular wall motion and myocardial perfusion with technetium-99m-methoxy isobutyl isonitrile at stress and rest in patients with angina: comparison with thallium-201 SPECT. *J Nucl Med* 1990;31:457–463.
5. Dondi M, Tartagni F, Fallani F, et al. A comparison of rest sestamibi and rest-redistribution thallium single photon emission tomography: possible implications for myocardial viability detection in infarcted patients. *Eur J Nucl Med* 1993;20:26–31.
6. Rigo P, Leclercq B, Itti R, et al. Technetium-99m-tetrofosmin myocardial imaging: a comparison with thallium-201 and angiography. *J Nucl Med* 1994;35:587–593.
7. Cuocolo A, Maurea S, Pace L, et al. Resting technetium-99m methoxy isobutylisonitrile cardiac imaging in chronic coronary artery disease: comparison with rest-redistribution thallium-201 scintigraphy. *Eur J Nucl Med* 1993;20:1186–1192.
8. Maurea S, Cuocolo A, Pace L, et al. Rest-injected thallium-201 redistribution and resting technetium-99m methoxyisobutylisonitrile uptake in coronary artery disease: relation to the severity of coronary artery stenosis. *Eur J Nucl Med* 1993;20:502–510.
9. Li ST, Liu XJ, Lu ZL, et al. Quantitative analysis of technetium-99m 2-methoxyisobutyl isonitrile single-photon emission computed tomography and isosorbide dinitrate infusion in assessment of myocardial viability before and after revascularization. *J Nucl Cardiol* 1996;3:457–463.
10. Eisner R, Tamas MJ, Cloninger K, et al. Normal SPECT thallium-201 bull's-eye display: gender differences. *J Nucl Med* 1988;29:1901–1909.
11. Tartagni F, Dondi M, Limonetti P, et al. Dipyridamole technetium-99m-2-methoxy isobutyl isonitrile tomoscintigraphic imaging for identifying diseased coronary vessels: comparison with thallium-201 stress-rest study. *J Nucl Med* 1991;32:369–376.
12. Maublant JC, Peycelon P, Kwiatkowski F, et al. Comparison between 180 degrees and 360 degrees data collection in technetium-99m MIBI SPECT of the myocardium. *J Nucl Med* 1989;30:295–300.
13. Benoit T, Vivegnis D, Foulon J, et al. Quantitative evaluation of myocardial single-photon emission tomographic imaging: application to the measurement of perfusion defect size and severity. *Eur J Nucl Med* 1996;23:1603–1612.
14. Sridhara BS, Braat S, Rigo P, et al. Comparison of myocardial perfusion imaging with technetium-99m tetrofosmin versus thallium-201 in coronary artery disease. *Am J Cardiol* 1993;72:1015–1019.
15. Martinez EE, Horowitz SF, Castello HJ, et al. Lung and myocardial thallium-201 kinetics in resting patients with congestive heart failure: correlation with pulmonary capillary wedge pressure. *Am Heart J* 1992;123:427–432.
16. Nordrehaug JE, Danielsen R, Vik-Mo H. Physiological inverse relationship between heart rate and thallium-201 lung uptake, clearance and lung/myocardial uptake ratio. *Eur Heart J* 1990;11:628–633.